

Quantitative Aspects of the Dynamical CPA in Harmonic Approximation

Toshihito TAMASHIRO, Shota NOHARA, Keisuke MIYAGI, and Yoshiro KAKEHASHI*

*Department of Physics and Earth Sciences, Faculty of Science, University of the Ryukyus,
1 Senbaru, Nishihara, Okinawa, 903-0213, Japan*

Magnetic and electronic properties of the Hubbard model on the Bethe and fcc lattices in infinite dimensions have been investigated numerically on the basis of the dynamical coherent potential approximation (CPA) theory combined with the harmonic approximation (HA) in order to clarify the quantitative aspects of the theory. It is shown that the dynamical CPA+HA reproduces well the sublattice magnetization, the magnetizations, susceptibilities, and the Néel temperatures (T_N) as well as the Curie temperatures calculated by the Quantum Monte-Carlo (QMC) method. The critical Coulomb interactions (U_c) for the metal-insulator (MI) transition are also shown to agree with the QMC results above T_N . Below T_N , U_c deviate from the QMC values by about 30% at low temperature regime. These results indicate that the dynamical CPA+HA is applicable to the quantitative description of the magnetic properties in high dimensional systems, but one needs to take into account higher-order dynamical corrections in order to describe the MI transition quantitatively at low temperatures.

KEYWORDS: Dynamical CPA, Curie temperature, Néel temperature, Effective Bohr magneton number, Metal-insulator transition, Excitation spectra, Hubbard model

1. Introduction

The magnetism of correlated electron systems with intermediate Coulomb interaction strength has been one of the long standing problems in the solid-state physics because these systems show the complex properties known as the itinerant vs. localized behaviors.^{1,2)} The ground-state magnetizations of Fe, Co, Ni, for example, show the noninteger values in unit of the Bohr magneton number being characteristic of a band model, while their finite-temperature properties such as the magnetization vs. temperature curves and the Curie-Weiss susceptibilities are well explained by a Heisenberg-type localized model. The Hartree-Fock theory and simple perturbation theories could not explain their magnetic properties since these theories overestimate the magnetic energy at finite temperatures.

Because of the difficulty in describing the itinerant vs. localized behavior in the magnetism of transition metals, interpolation theories have been developed by many investigators. Cyrot³⁾ adopted the functional integral method⁴⁾ to the Hubbard model and derived the P - T phase diagram of metal-insulator (MI) phase transition at finite temperatures. Hubbard⁵⁾ and Hasegawa⁶⁾ independently developed the single-site spin fluctuation theory (SSF) on the basis of the functional integral method. The theory transforms the electron-electron interaction into a time-dependent random potential by introducing the time-dependent charge and exchange random fictitious field variables, and treats the potentials using the coherent potential approximation (CPA).⁷⁾ The theory interpolates between the weak and strong Coulomb interaction limits, and explained qualitatively the localized vs. itinerant behaviors of magnetism in transition metals.

The SSF is based on the static approximation (SA)

which neglects the time dependence of the fictitious fields. Though the SA is exact in the high temperature limit, it reduces to the Hartree-Fock theory at the ground state. Thus it does not take into account the electron correlations as found at the zero temperature by Gutzwiller,⁸⁾ Hubbard,⁹⁾ and Kanamori.¹⁰⁾ Kakehashi and Fulde¹¹⁾ proposed a variational theory at finite temperatures which takes into account the ground-state electron correlations, and showed that the correlations at finite temperatures can reduce the Curie temperatures obtained by the SSF by a factor of two.

Towards more quantitative theory, Kakehashi¹²⁾ proposed the dynamical CPA which completely takes into account electron correlations at finite temperatures within the single-site approximation, and clarified the basic properties of the theory using a Monte-Carlo technique. Later he proposed an analytic theory of the dynamical CPA combined with the harmonic approximation (HA),¹³⁾ and examined the dynamical effects on the itinerant ferromagnetism. In the HA,¹⁴⁾ we neglect the mode-mode couplings between the dynamical potentials, and take into account the contributions from the dynamical potentials with the same frequency independently. The HA is known to be exact up to the second order in the weak Coulomb interaction limit, and is known to describe quantitatively the Kondo limit in the strong Coulomb interaction regime.¹⁵⁾ The dynamical CPA has recently been proved^{2,16)} to be equivalent to the many-body CPA in the disordered problem,¹⁷⁾ the dynamical mean-field theory in the metal-insulator transition in infinite dimensions,¹⁸⁾ and the projection-operator method CPA for excitations in solids.¹⁹⁾

More recently, we proposed the first-principles dynamical CPA²⁰⁾ on the basis of the tight-binding linear muffintin orbital (TB-LMTO) Hamiltonian^{21,22)} with the LDA (Local Density Approximation)+ U type in-

*E-mail address: yok@sci.u-ryukyu.ac.jp, to be published in J. Phys. Soc. Jpn.

traatomic Coulomb interactions,²³⁾ and clarified the ferromagnetism of Fe, Co, and Ni,^{24,25)} as well as the systematic change of excitation spectra in 3d transition metal series.^{26,27)}

Although the numerical results of the first-principles dynamical CPA combined with the HA seem to be reasonable and explained well a systematic change of the XPS and BIS data,²⁶⁾ the validity of the dynamical CPA+HA has not yet been examined in details. The purpose of the present paper is to clarify the quantitative aspects of the dynamical CPA+HA from the numerical point of view. For this purpose, we have calculated the antiferromagnetic properties of the half-filled Hubbard model on the Bethe lattice in infinite dimensions¹⁸⁾ and the ferromagnetic properties of the non half-filled Hubbard model on the fcc lattice in infinite dimensions²⁸⁾ on the basis of the dynamical CPA+HA. We clarify the validity of the theory by comparing the results of calculations with those of the Quantum Monte-Carlo (QMC) method.²⁹⁻³³⁾ We will conclude that the dynamical CPA approach is useful for the quantitative understanding of the magnetic properties of solids in high dimensions where the single-site approximation works well.

Outline of the present paper is as follows. In §2, we summarize the dynamical CPA combined with the HA and extend the theory to the antiferromagnetic case with the bipartite lattice. In §3.1 we present the results of calculations for the antiferromagnetic states in the half-filled Hubbard model on the Bethe lattice. It is shown that the zeroth approximation to the dynamical CPA, *i.e.*, the SA quantitatively describes the Néel temperatures (T_N) as well as the MI boundary above T_N . We present in §3.2 the results of calculations for the densities of states (DOS) as well as the MI transition below T_N . We will show that the dynamical effects tend to increase the critical Coulomb interaction for the MI transition. The numerical results for the ferromagnetic properties on the fcc lattice in infinite dimensions are presented in §3.3. The Curie temperatures as well as the paramagnetic susceptibilities are shown to be described quantitatively by means of the dynamical CPA+HA in the quarter-filled regime of electron number. In the last §4 we summarize our numerical results. It is emphasized that the dynamical CPA is applicable to the quantitative description of the magnetic properties in high dimensions.

2. Dynamical CPA in the ferro- and antiferromagnetic states

We adopt in the present paper the Hubbard model as follows.

$$\hat{H} = \sum_{i,\sigma} \epsilon_0 n_{i\sigma} + \sum_{i,j,\sigma} t_{ij} a_{i\sigma}^\dagger a_{j\sigma} + \sum_i U n_{i\uparrow} n_{i\downarrow}. \quad (1)$$

Here ϵ_0 is the atomic energy level, t_{ij} is the transfer integrals between sites i and j , and U is the intraatomic Coulomb interaction energy parameter. $a_{i\sigma}^\dagger$ ($a_{i\sigma}$) denotes the creation (annihilation) operator for an electron with spin σ on site i , and $n_{i\sigma} = a_{i\sigma}^\dagger a_{i\sigma}$ is the number operator for the electron.

In the dynamical CPA,¹³⁾ we transform the two-body

interaction $U n_{i\uparrow} n_{i\downarrow}$ in the free energy into a dynamical one-body potential v_i with time-dependent random spin and charge fields using the Hubbard-Stratonovich transformation.³⁴⁾ Then introducing the site-diagonal effective potential Σ_i (*i.e.*, the coherent potential) into the potential part of the free energy, we expand the correction terms containing $v_i - \Sigma_i$ with respect to the site. The zeroth term is the coherent term $\tilde{\mathcal{F}}[\Sigma]$ which does not depend on the dynamical potential at all. The next term consists of the single-site terms each of which contains the dynamical potential on the same site. The higher-order terms $\Delta\mathcal{F}$ describe the inter-site spin and charge fluctuations.

In the dynamical CPA, we adopt the single-site approximation which neglects the higher-order inter-site corrections $\Delta\mathcal{F}$. The free energy of the dynamical CPA is then written as follows.

$$\mathcal{F}_{\text{CPA}} = \tilde{\mathcal{F}}[\Sigma] - \beta^{-1} \sum_i \ln \int \sqrt{\frac{\beta U}{4\pi}} d\xi_i e^{-\beta E^{(i)}(\xi_i)}. \quad (2)$$

Here β denotes the inverse temperature, ξ_i is the static exchange field on site i , and $E^{(i)}(\xi_i)$ is a single-site effective potential projected onto the static field ξ_i .

The effective potential $E^{(i)}(\xi)$ consists of the static part $E_{\text{st}}^{(i)}(\xi)$ and the dynamical part $E_{\text{dyn}}^{(i)}(\xi)$.

$$E^{(i)}(\xi) = E_{\text{st}}^{(i)}(\xi) + E_{\text{dyn}}^{(i)}(\xi). \quad (3)$$

The static potential $E_{\text{st}}^{(i)}(\xi)$ is obtained by neglecting the time-dependence of the field variables and is given by

$$E_{\text{st}}^{(i)}(\xi) = -\frac{1}{\beta} \sum_{l,\sigma} \ln [1 - (v_{i\sigma}^{(0)}(\xi) - \Sigma_{i\sigma}(i\omega_l)) F_{i\sigma}(i\omega_l)] - \frac{1}{4} U (\tilde{n}_i(\xi)^2 - \xi^2), \quad (4)$$

$$v_{i\sigma}^{(0)}(\xi) = \epsilon_0 - \mu + \frac{1}{2} U \tilde{n}_i(\xi) - \frac{1}{2} U \xi \sigma. \quad (5)$$

Here $v_{i\sigma}^{(0)}(\xi)$ is the Hartree-Fock type static potential. μ denotes the chemical potential. $\Sigma_{i\sigma}(i\omega_l)$ is the frequency representation of a time-dependent coherent potential $\Sigma_{i\sigma}(\tau)$, τ being the imaginary time. $\omega_l = (2l+1)\pi/\beta$ denotes the Matsubara frequency. The electron number $\tilde{n}_i(\xi)$ for a given exchange field ξ is defined by

$$\tilde{n}_i(\xi) = \frac{1}{\beta} \sum_{l,\sigma} G_{i\sigma}(i\omega_l, \xi). \quad (6)$$

The Green function $G_{i\sigma}(i\omega_l, \xi)$ will be determined later self-consistently (see eq. (16)).

The coherent Green function $F_{i\sigma}(i\omega_l)$ in eq. (4) is defined by

$$F_{i\sigma}(i\omega_l) = [(i\omega_l - \mathbf{H}_0 - \Sigma_{i\sigma}(i\omega_l))^{-1}]_{ii}. \quad (7)$$

Here $(\mathbf{H}_0)_{ij} = (\epsilon_0 - \mu)\delta_{ij} + t_{ij}(1 - \delta_{ij})$ is the one-electron Hamiltonian matrix element in eq. (1) and $(\Sigma_{i\sigma}(i\omega_l))_{ij} = \Sigma_{i\sigma}(i\omega_l)\delta_{ij}$.

The dynamical potential $E_{\text{dyn}}^{(i)}(\xi)$ in eq. (3) is given in

the harmonic approximation (HA) as

$$E_{\text{dyn}}^{(i)}(\xi) = -\frac{1}{\beta} \ln \left[1 + \sum_{\nu=1}^{\infty} \sum_{n=1}^{\infty} \overline{D}_{i\nu}^{(n)} \right], \quad (8)$$

$$\overline{D}_{i\nu}^{(n)} = U^{2n} \left(\frac{i}{2\pi\nu} \right)^{2n} B_{i\nu\uparrow}^{(n)} B_{i\nu\downarrow}^{(n)}. \quad (9)$$

First few terms of $B_{i\nu\sigma}^{(n)}$ are given as follows.¹³⁾

$$B_{i\nu\sigma}^{(1)} = \frac{2\pi i\nu}{\beta} \sum_{l=0}^{\infty} \left(\tilde{g}_{i\sigma}(l-\nu) \tilde{g}_{i\sigma}(l) + \tilde{g}_{i\sigma}(l+\nu) \tilde{g}_{i\sigma}(l) \right)^*, \quad (10)$$

$$B_{i\nu\sigma}^{(2)} = \left(\frac{2\pi\nu}{\beta} \right)^2 \text{Re} \left[2 \sum_{l=0}^{\infty} \tilde{g}_{i\sigma}(l-\nu) \tilde{g}_{i\sigma}(l) \times \left(\tilde{g}_{i\sigma}(l-2\nu) \tilde{g}_{i\sigma}(l-\nu) + \tilde{g}_{i\sigma}(l-\nu) \tilde{g}_{i\sigma}(l) + \tilde{g}_{i\sigma}(l) \tilde{g}_{i\sigma}(l+\nu) - \sum_{l=0}^{\nu-1} (\tilde{g}_{i\sigma}(l-\nu) \tilde{g}_{i\sigma}(l))^2 \right) \right] + B_{i\nu\sigma}^{(1)2}. \quad (11)$$

Here $\tilde{g}_{i\sigma}(l)$ is the static Green function on site i , which is defined by

$$\tilde{g}_{i\sigma}(l) = [F_{i\sigma}(i\omega_l)^{-1} - v_{i\sigma}^{(0)}(\xi) + \Sigma_{i\sigma}(i\omega_l)]^{-1}. \quad (12)$$

For the higher-order terms of $B_{i\nu\sigma}^{(n)}$, one can adopt the following form of the asymptotic approximation.

$$B_{i\nu\sigma}^{(n)} = \sum_{k=0}^{\nu-1} \frac{n!}{k!} \left[\prod_{k=0}^{\nu-1} B_{i\nu\sigma}^{(k)}(k) \right], \quad (13)$$

$$B_{i\nu\sigma}^{(l)}(k) = b_{l\sigma}^{(0)}(\nu, k) + \sum_{m=0}^{l-1} (-)^{l-m} \binom{l}{m} \times \left[b_{m\sigma}^{(0)}(\nu, k) b_{l-m\sigma}^{(0)}(-\nu, k) + \frac{2\pi(l-m)\nu}{i\beta} \tilde{g}_{i\sigma}(-\nu+k) \tilde{g}_{i\sigma}(k) \times b_{m\sigma}^{(1)}(\nu, k) b_{l-m-1\sigma}^{(1)}(-\nu, k) \right]. \quad (14)$$

The functions $b_{m\sigma}^{(0)}(\pm\nu, k)$ and $b_{m\sigma}^{(1)}(\pm\nu, k)$ in the 0-th order and the second order asymptotic approximation are given in Appendix B of Ref.¹³⁾

The coherent potential $\Sigma_{i\sigma}(i\omega_l)$ is determined so that the higher-order inter-site corrections become minimum. The condition called the CPA equation is given by

$$\langle G_{i\sigma}(i\omega_l, \xi) \rangle_{\text{eff}} = F_{i\sigma}(i\omega_l). \quad (15)$$

Here the average $\langle \rangle_{\text{eff}}$ at the l.h.s. (left-hand-side) of the above equation means taking a classical average with respect to the effective potential $E^{(i)}(\xi)$. The on-site dy-

namical impurity Green function is given by

$$G_{i\sigma}(i\omega_l, \xi) = \tilde{g}_{i\sigma}(l) + \frac{\sum_{\nu=1}^{\infty} \sum_{n=1}^{\infty} \frac{\delta \overline{D}_{i\nu}^{(n)}}{\kappa_{i\sigma}(i\omega_l) \delta \Sigma_{i\sigma}(i\omega_l)}}{1 + \sum_{\nu=1}^{\infty} \sum_{n=1}^{\infty} \overline{D}_{i\nu}^{(n)}}. \quad (16)$$

Here $\kappa_{i\sigma}(i\omega_l) = 1 - F_{i\sigma}(i\omega_l)^{-2} \delta F_{i\sigma}(i\omega_l) / \delta \Sigma_{i\sigma}(i\omega_l)$.

The average electron number $\langle n_i \rangle$ and the local magnetic moment $\langle m_i \rangle$ are given by

$$\langle n_i \rangle = \langle \tilde{n}_i(\xi_i) \rangle_{\text{eff}}, \quad (17)$$

$$\langle m_i \rangle = \langle \xi_i \rangle_{\text{eff}}. \quad (18)$$

The double occupation number $\langle n_{i\uparrow} n_{i\downarrow} \rangle$ and the amplitudes of local moment on site i are obtained from the following expressions.¹³⁾

$$\langle n_{i\uparrow} n_{i\downarrow} \rangle = \frac{1}{4} \langle \tilde{n}_i(\xi_i)^2 \rangle_{\text{eff}} - \frac{1}{4} \left(\langle \xi_i^2 \rangle_{\text{eff}} - \frac{2}{\beta U} \right) + \left\langle \left[\frac{\partial E_{\text{dyn}}^{(i)}(\xi_i)}{\partial U} \right]_v \right\rangle_{\text{eff}}, \quad (19)$$

$$\langle m_i^2 \rangle = \langle n_i \rangle - 2 \langle n_{i\uparrow} n_{i\downarrow} \rangle. \quad (20)$$

Here $[\]_v$ means to take the derivative of a quantity fixing the static potential $v_{i\sigma}^{(0)}(\xi_i)$.

Equations (15) and (17) form a set of self-consistent equations to determine the coherent potential $\{\Sigma_{i\sigma}(i\omega_l)\}$ and the chemical potential $\epsilon_0 - \mu$. However it is time consuming to solve the CPA equation (15) because one has to take the average $\langle \rangle_{\text{eff}}$ at each frequency ω_l . The following decoupling approximation simplifies the numerical calculations.

$$\sum_{q=\pm 1} \frac{1}{2} \left(1 + q \frac{\langle \xi_i \rangle_{\text{eff}}}{x_i} \right) G_{i\sigma}(i\omega_l, qx_i) = F_{i\sigma}(i\omega_l). \quad (21)$$

Here $x_i = \sqrt{\langle \xi_i^2 \rangle_{\text{eff}}}$. Note that the approximation is correct up to the second moment (*i.e.*, $\langle \xi_i \rangle_{\text{eff}}$ and $\langle \xi_i^2 \rangle_{\text{eff}}$).

We assume in this work that each site is crystallographically equivalent to each other. In the para- and ferro-magnetic states, we can assume a site-independent coherent potential $\Sigma_{\sigma}(i\omega_l)$. The site-independent coherent Green function $F_{\sigma}(i\omega_l)$ is then given by

$$F_{\sigma}(i\omega_l) = \int \frac{\rho(\epsilon) d\epsilon}{i\omega_l - \epsilon_0 + \mu - \Sigma_{\sigma}(i\omega_l) - \epsilon}. \quad (22)$$

Here $\rho(\epsilon)$ is the density of states (DOS) for the noninteracting Hamiltonian matrix t_{ij} .

In the antiferromagnetic state with sublattice magnetization, we have two types of coherent potential; $\Sigma_{\sigma}^{(+)}(i\omega_l)$ on the up-spin sublattice and $\Sigma_{\sigma}^{(-)}(i\omega_l)$ on the down-spin sublattice. Because of the symmetric relation $\Sigma_{\sigma}^{(-)}(i\omega_l) = \Sigma_{-\sigma}^{(+)}(i\omega_l)$, it is enough to require the self-consistency of $\Sigma_{\sigma}^{(+)}(i\omega_l)$ on the up-spin sublattice. The corresponding coherent Green function $F_{\sigma}^{(+)}(i\omega_l)$ is given

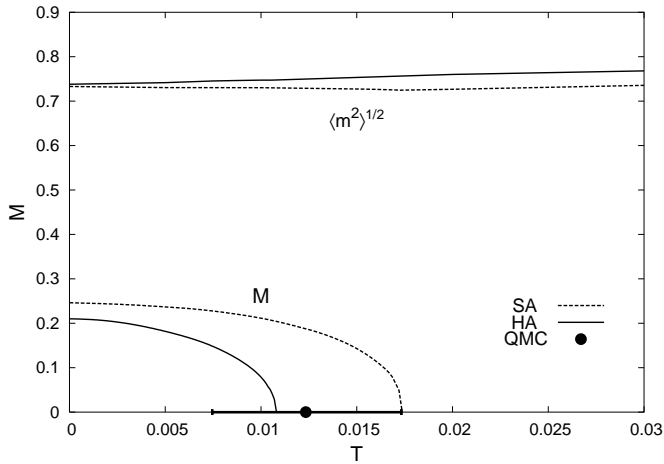


Fig. 1. Sublattice magnetization vs. temperature curves and the amplitude of local moments $\langle m^2 \rangle^{1/2}$ for the half-filled Hubbard model on the Bethe lattice in infinite dimensions. Coulomb interaction energy parameter is chosen to be $U = 0.5$ in unit of half the band width for noninteracting density of states. Dashed curves show the results of the static approximation (SA), solid curves show the results of the harmonic approximation (HA), closed circle with error bar indicates the Néel temperature obtained by the Quantum Monte-Carlo (QMC) method.^{29,30}

by^{35,36})

$$F_{\sigma}^{(+)}(i\omega_l) = \sqrt{\frac{i\omega_l - \Sigma_{-\sigma}^{(+)}(i\omega_l)}{i\omega_l - \Sigma_{\sigma}^{(+)}(i\omega_l)}} \times \int \frac{\rho(\epsilon)d\epsilon}{\sqrt{(i\omega_l - \Sigma_{+}^{(+)}(i\omega_l))(i\omega_l - \Sigma_{-}^{(+)}(i\omega_l)) - \epsilon_0 + \mu - \epsilon}}. \quad (23)$$

We adopted eqs. (22) and (23) in the para- and antiferro-magnetic calculations on the Bethe lattice and in the ferromagnetic calculations on the fcc lattice in infinite dimensions. Moreover in the self-consistent calculations with use of the HA, we adopted eqs. (10) and (11) for U^2 and U^4 terms and took into account the higher-order terms up to U^{16} using the asymptotic approximation, *i.e.* eqs. (13) and (14).

3. Numerical Results

3.1 Antiferromagnetic states on the Bethe lattice

We present in this subsection the numerical results of calculations for the antiferromagnetic states at half filling on the Bethe lattice in infinite dimensions. The DOS for the noninteracting system is given by a semi-elliptical form as

$$\rho(\epsilon) = \frac{2}{\pi W^2} \sqrt{W^2 - \epsilon^2}. \quad (24)$$

Here $2W$ denotes the band width. In the present and next subsections, we adopt the energy unit to be $W = 1$.

We found that the antiferromagnetism is stabilized at half filling with decreasing temperatures. The numerical results of sublattice magnetization vs. temperature curves are presented in Fig. 1 for rather small Coulomb interaction energy parameter $U = 0.5$. Calculated Néel

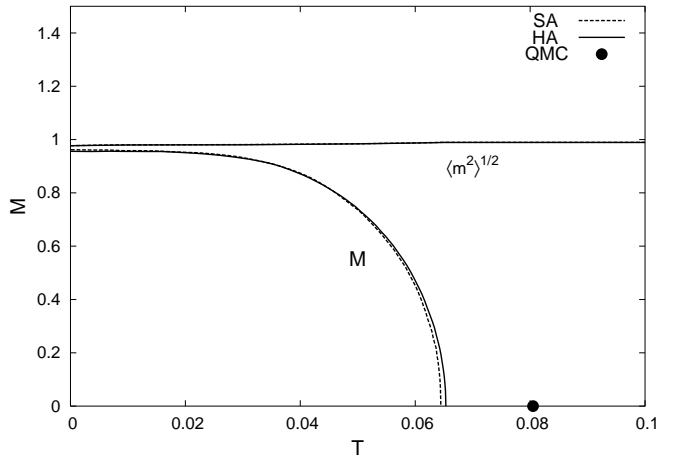


Fig. 2. Sublattice magnetization vs. temperature curves and the amplitude of local moments for $U = 3.5$. Notations are the same as in Fig. 1.

temperatures T_N are 0.017 in the static approximation (SA) and 0.011 in the harmonic approximation (HA), respectively. The dynamical effects reduce the ground-state sublattice magnetization (extrapolated value) by 15% and T_N by 36%. The calculated Néel temperature with dynamical corrections seems to be in good agreement with the QMC result as shown in Fig. 1. Although the agreement might not be so convincing because of a large error bar in the QMC calculations, quantitative description in the weak Coulomb interaction regime is expected because the HA is exact up to the second order in U in the weak Coulomb interaction limit. The amplitude of local moment $\langle m^2 \rangle^{1/2}$ is also enhanced by the dynamical effects because electron correlations suppress the double occupancy of electrons even at finite temperatures.

The results for a strong Coulomb interaction $U = 3.5$ are presented in Fig. 2. The sublattice magnetization and Néel temperature are much enhanced as compared with the case of $U = 0.5$. The ground-state sublattice magnetization ($0.960 \mu_B$ for the SA and $0.955 \mu_B$ in the HA) is close to the atomic value $1.0 \mu_B$. Calculated T_N are 0.0645 in the SA and 0.0654 in the HA, respectively; the T_N is slightly increased by the dynamical effects, but is smaller than the QMC value²⁹) by 18%.

We have calculated the Néel temperatures for various Coulomb interaction energy parameters. The results are summarized in Fig. 3. It should be noted that we adopted the decoupling approximation (21) in the calculations of Figs. 1 and 2 in order to reduce the computation time. To clarify the difference between the decoupling approximation (21) and the full self-consistent CPA (15), we performed the full static calculations with use of (15). The calculated T_N vs. U curve is shown by solid curve and is compared with those in the decoupling approximation as well as the QMC results. In both the weak and strong Coulomb interaction regimes (*i.e.*, $U < 1$ and $U > 3$), calculated T_N with different approximation schemes yield basically the same result. In the intermediate Coulomb interaction regime (*i.e.*, $1 < U < 3$), the Néel tempera-

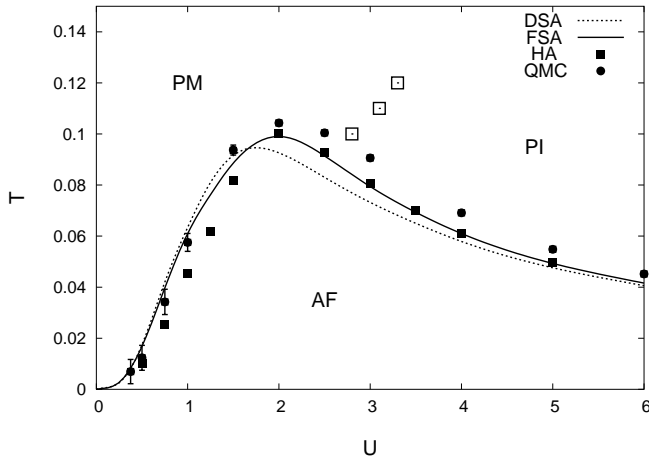


Fig. 3. Néel temperatures (T_N) in the SA with decoupling approximation (dotted curve), the full SA (solid curve), the HA with dynamical corrections (closed squares), and the QMC method (closed circles).^{29, 30} The open squares around $U = 3.0$ above T_N indicate the metal-insulator crossover points in the full SA. Below T_N , the antiferromagnetic state (AF) is stabilized, while above T_N the paramagnetic metal (PM) and the paramagnetic insulator (PI) are realized.

tures in the decoupling approximation deviate from the full static results by several percent. It should be noted that T_N calculated by the full SA quantitatively agree with the QMC results. This indicates that the SA provides us with a good starting point to calculate quantitatively the magnetic properties of electrons especially at high temperatures.

We have estimated the Néel temperatures in the full HA by adding $\Delta T_N = T_N(\text{HA}) - T_N(\text{SA})$ in the decoupling approximation to T_N in the full static one.³⁷ The results are shown in Fig. 3 by closed squares. We find that the dynamical effects in the harmonic approximation reduce T_N in the weak Coulomb interaction regime ($U < 1$) and slightly increase T_N in the strong Coulomb interaction regime ($U > 2$). Calculated T_N are in agreement with the QMC results in the weak U regime, but are underestimated in the intermediate and strong U regimes ($1 \lesssim U$). In particular the present dynamical calculations hardly correct T_N in the SA in the strong U regime ($2 \lesssim U$). One of the possible reasons for insufficient corrections is that the decoupling approximation is not suitable at high temperatures; it tends to overestimate the magnetic entropy at high temperatures because the approximation implies to replace a broad distribution $p(\xi) = \exp(-\beta E^{(i)}(\xi)) / \int d\xi \exp(-\beta E^{(i)}(\xi))$ with a two-delta function. The higher order dynamical corrections should also be taken into account in eq. (9) for strong U regime in order to make more reasonable corrections.

3.2 Metal-insulator transition

Single-particle excitation spectra are obtained by means of a numerical analytic continuation³⁸ of the self-energy for temperature Green function, *i.e.*, the coherent potential $\Sigma_{i\sigma}(i\omega)$. It should be noted that the coherent potential obtained by solving the CPA equation (21) in the decoupling approximation is an approximate solution

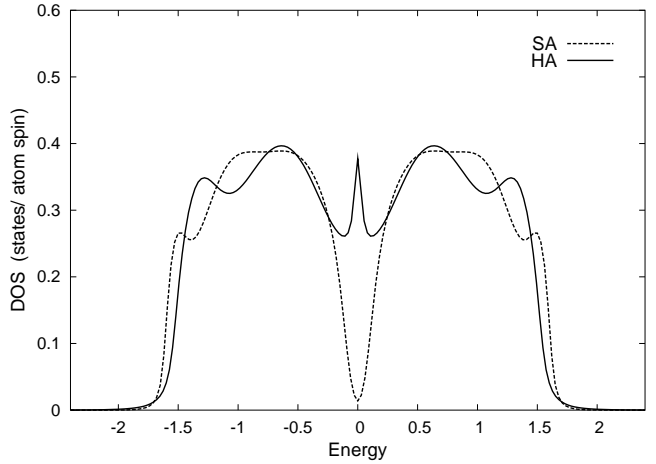


Fig. 4. Density of states (DOS) for $U = 1.7$ and $T = 0.06$ in the SA (dashed curve), and in the HA with dynamical corrections (solid curve).

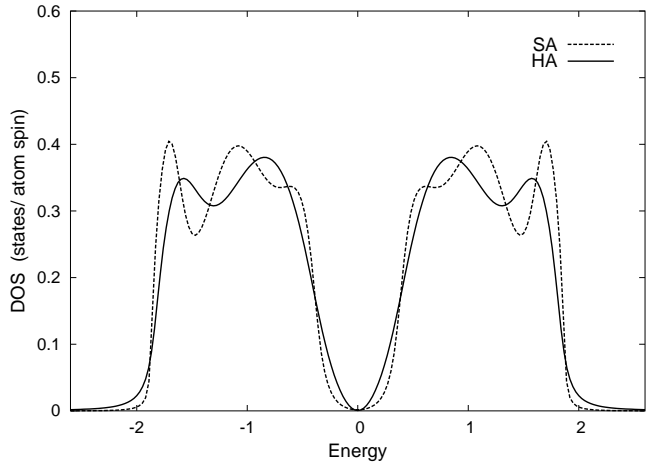


Fig. 5. DOS for $U = 2.2$ and $T = 0.06$ in the SA (dashed curve), and in the HA with dynamical corrections (solid curve).

to the full equation (15). In order to obtain accurately the DOS as the single-particle excitations, we improved the coherent potential adopting the average t -matrix approximation (ATA)^{7, 39} after we solved eq. (21).

$$\Sigma_{i\sigma}^{\text{ATA}}(i\omega_n) = \Sigma_{i\sigma}(i\omega_n) + \frac{\langle G_{i\sigma}(i\omega_n, \xi) \rangle_{\text{eff}} - F_{i\sigma}(i\omega_n)}{\langle G_{i\sigma}(i\omega_n, \xi) \rangle_{\text{eff}} F_{i\sigma}(i\omega_n)}. \quad (25)$$

Here the coherent potential in the decoupling approximation was used at the r.h.s. (right-hand-side) of the above equation, but the full average $\langle \rangle_{\text{eff}}$ of the impurity Green function is taken. The ATA is a one-shot correction to the full CPA (15).

Making use of the Padé numerical analytic continuation,³⁸ we obtained $\Sigma_{i\sigma}^{\text{ATA}}(\omega + i\delta)$. Here ω is an energy variable on the real axis and δ is an infinitesimal positive number. Using the self-energy, we obtained the coherent Green function $F_{i\sigma}^{(+)}(\omega + i\delta)$, and calculated the DOS via the relation,

$$\rho_{\sigma}(\omega) = -\frac{1}{\pi} \text{Im} F_{i\sigma}^{(+)}(\omega + i\delta). \quad (26)$$

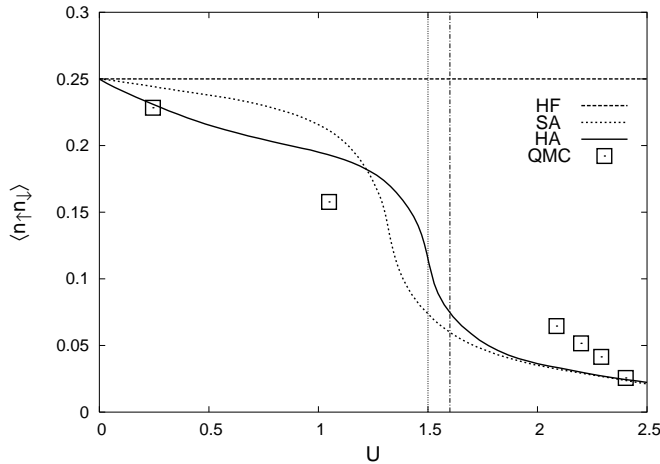


Fig. 6. Double occupation numbers as a function of U at $T = 0.02$ in the Hartree-Fock (HF) approximation (dashed curve), the SA (dotted curve), and the HA (solid curve). The paramagnetic state is assumed. Open squares show the double occupation numbers in the QMC calculations¹⁸⁾ at $T = 0.03125$. The vertical lines indicate the critical Coulomb interaction U_c in the SA ($U_c = 1.5$: thin dotted line) and HA ($U_c = 1.6$: dot-dashed line). Both values of U_c are obtained within the decoupling approximation (21).

The system changes from metal to insulator with the formation of a gap on the Fermi level with increasing Coulomb interaction. In the full SA, the gap is gradually formed above the Néel temperatures. The crossover points are shown in Fig. 3 by open squares. When we assume the paramagnetic state below T_N , the formation of a gap becomes clearer at lower temperatures, indicating the metal-insulator (MI) transition.

Figure 4 shows the DOS in the metallic state near the MI transition. We find the upper and lower Hubbard bands. A gap is almost opened on the Fermi level in the SA, while the quasiparticle peak remain in the dynamical calculations. When the Coulomb interaction energy U is increased, a gap is opened as shown in Fig. 5. The dynamical effects shift the spectral weight to the lower energy region.

The metal-insulator transition is accompanied by a localization of electrons. We show in Fig. 6 an example of double occupation number $\langle n_{\uparrow}n_{\downarrow} \rangle$ vs U curve at low temperatures. The Hartree-Fock approximation yields the constant value 0.25 irrespective of U because of no on-site correlations. The double occupation number in the SA reduces to the Hartree-Fock value in the weak Coulomb interaction limit. It rapidly decreases near the MI transition, and gives the alloy-analogy results of the Hubbard theory⁹⁾ in the strong U limit. The dynamical effects based on the HA reduce further the double occupancy in the weak U regime and enhance it in the strong U regime as shown in Fig. 6.

There are no QMC calculations on the double occupation number at $T = 0.02$. We plotted in Fig. 6 the QMC results¹⁸⁾ at $T = 0.031$ for qualitative or semi-quantitative comparison with the present results. The QMC value at $U = 0.25$ indicates that the dynamical CPA+HA yields the quantitative result in the weak

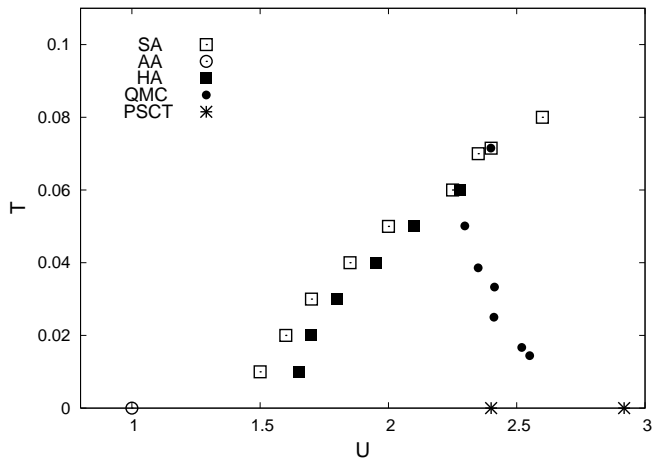


Fig. 7. Phase boundaries of metal-insulator transition below T_N in the SA (open squares), the HA (closed squares), and the QMC method (closed circles).³¹⁾ The critical Coulomb interaction in the alloy-analogy approximation (AA)⁹⁾ at $T = 0$ is indicated by the open circle, while the exact results of U_{c1} and U_{c2} at $T = 0$ based on the projective self-consistent technique (PSCT)³²⁾ are indicated by the stars.

Coulomb interaction. The QMC result at $U = 1.0$ suggests that the HA is not sufficient to reduce the double occupancy in the intermediate regime of the Coulomb interaction. It should be noted that the critical Coulomb interaction in the QMC is $U_c = 2.4$ so that the data in $2.0 < U < 2.4$ are for metallic region. Thus, they are not directly compared with the present results in the insulator regime. The dynamical CPA+HA result at $U = 2.4$ agrees with the QMC result. These results suggest that the HA gives the quantitative results of $\langle n_{\uparrow}n_{\downarrow} \rangle$ in both the weak ($U < 1.0$) and strong ($U > 2.4$) Coulomb interaction regimes. In the intermediate Coulomb interaction regime ($1.0 \lesssim U \lesssim 2.3$), we need to take into account more dynamical effects to obtain $\langle n_{\uparrow}n_{\downarrow} \rangle$ quantitatively at low temperatures.

We have plotted in Fig. 7 the MI transition points below T_N being obtained from the gap formation in the DOS. The critical Coulomb interactions U_c for gap formation in the full SA increase with increasing temperature, and merge into the QMC results³¹⁾ around $T \approx 0.06$. Since the full SA is exact in the high temperature limit, this indicates that the full SA quantitatively describes U_c at $T > 0.06$. It should be noted that these data are smoothly connected to the data points above T_N for a gap formation in Fig. 3. Below $T = 0.06$, the U_c in the SA deviate from the QMC results, and reduces to $U_c = 1.0$ in the Hubbard alloy-analogy approximation⁹⁾ at $T = 0$.

The dynamical results of U_c in Fig. 7 are obtained by adding the dynamical correction $\Delta U_c = U_c(\text{HA}) - U_c(\text{SA})$ in the decoupling approximation to $U_c(\text{SA})$ in the full SA.³⁷⁾ It is known that there are two critical Coulomb interactions at $T = 0$, U_{c1} for the gap formation and U_{c2} for the disappearance of the quasiparticle state.¹⁸⁾ But we did not find numerically two solutions near U_c at finite temperatures ($T > 0.01$). The critical

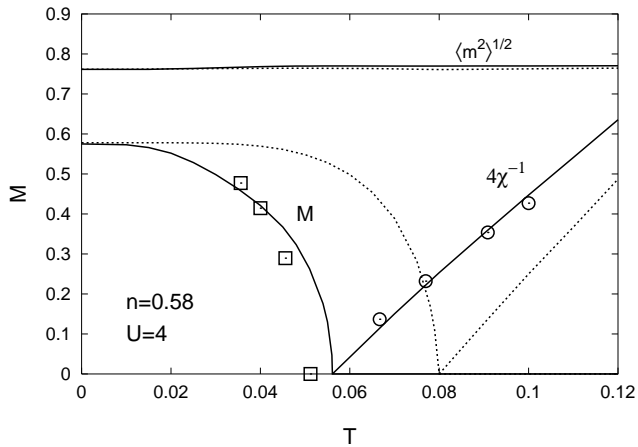


Fig. 8. Magnetization (M), inverse susceptibility (χ^{-1}) and amplitude of local moment ($\langle m^2 \rangle^{1/2}$) as a function of temperature (T) on the fcc lattice in infinite dimensions. Solid curves: dynamical CPA+HA, dotted curves: dynamical CPA+SA. Open squares (open circles) are the magnetizations (inverse susceptibilities) in the QMC.³³⁾

Coulomb interactions in the HA are larger than those of the full static approximation. The difference between the two becomes smaller with increasing temperature and vanishes at $T > 0.06$ as it should be. The critical Coulomb interaction extrapolated to the zero temperature is about 1.6 in the present HA, while the exact values based on the projective self-consistent technique (PSCT)³²⁾ are reported to be $U_{c1} = 2.40$ and $U_{c2} = 2.84$. One has to take into account the dynamical terms higher than U^4 more seriously in order to describe the MI transition quantitatively.

3.3 Ferromagnetism on the fcc lattice in infinite dimensions

We have investigated the ferromagnetic properties of the fcc lattice in infinite dimensions by means of the dynamical CPA+HA in order to examine the quantitative aspects of the theory. The fcc lattice in d dimensions is defined as a lattice with $2d(d-1)$ nearest neighbors expressed by $\mathbf{R} = \pm \mathbf{e}_i \pm \mathbf{e}_j$ with two different cubic unit vectors \mathbf{e}_i and \mathbf{e}_j ($i, j = 1, 2, \dots, d$). In infinite dimensions the noninteracting DOS is given by²⁸⁾

$$\rho(\epsilon) = \frac{e}{\sqrt{\pi(1 + \sqrt{2}\epsilon)}} \frac{(1 + \sqrt{2}\epsilon)}{2}. \quad (27)$$

Here the energy unit is chosen so that the bottom of band edge is given by $-1/\sqrt{2}$.

Note that the DOS (27) monotonically increases with decreasing energy ϵ and diverges at the band edge $\epsilon = -1/\sqrt{2}$. Therefore the DOS is expected to be favorable for the ferromagnetism in the low density region. Since the numerator in the DOS is reduced by a factor of $1/e$ at $\epsilon = 1/\sqrt{2}$, we may regard $W = \sqrt{2}$ as a characteristic band width of this system. The coherent Green function $F_\sigma(i\omega_l)$ was calculated from eq. (22) via numerical integration with respect to energy ϵ .

Figure 8 shows an example of calculated magnetization vs temperature curves in various approximations for electron number $n = 0.58$ and Coulomb interaction $U = 4.0$. Extrapolated ground-state magnetizations are almost saturated in both calculations. The magnetization vs. temperature curves considerably deviate downwards from the Brillouin curve. The SA overestimates the Curie temperature ($T_C = 0.0800$) as compared with the QMC³³⁾ ($T_C = 0.0512$). The dynamical effects based on the HA reduces T_C by 30% and results in $T_C = 0.0559$. The result agrees with the QMC³³⁾ ($T_C = 0.0512$) within 9% error. We have also calculated the paramagnetic susceptibilities above T_C by adding the infinitesimal magnetic field. Calculated susceptibilities follow the Curie-Weiss law; $\chi = m_{\text{eff}}^2/(T - T_C)$. Here m_{eff} is a constant called effective Bohr magneton number. Calculated effective Bohr magneton numbers are $1.00 \mu_B$ in the SA, $1.13 \mu_B$ in the HA, and $1.18 \mu_B$ in the QMC, respectively. We find a good agreement between the dynamical CPA+HA results and the QMC ones.

We have calculated T_C as a function of electron number n by extrapolating the inverse susceptibilities to lower temperatures at various n . The results are presented in Figs. 9 and 10 for an intermediate Coulomb interaction strength $U = 2$ and a strong Coulomb interaction $U = 4$, respectively. In the SA, we obtain a finite value of T_C for infinitesimal electron number n . The T_C increases linearly with increasing n , and shows a maximum $T_C = 0.053$ (0.083) at $n_{\text{max}} = 0.60$ (0.70) for $U = 2$ ($U = 4$). When electron number n approaches to one, T_C vanishes again at $n = 0.93$ (0.98) for $U = 2$ ($U = 4$). The dynamical effects reduce T_C , for example, by 35 % (25 %) at $n_{\text{max}} = 0.60$ (0.70) for $U = 2$ ($U = 4$). As shown in Figs. 9 and 10, the dynamical results quantitatively agree with the QMC results around the quarter filled electron number (*i.e.*, $0.4 \lesssim n \lesssim 0.6$) for both $U = 2$ and $U = 4$. However, the T_C vs n curves shift to the higher density region by about $\Delta n = 0.1$; calculated T_C in the low density regime ($0 < n \lesssim 0.3$) are underestimated, and those in the half-filled regime ($0.7 \lesssim n < 1$) are overestimated.

The behavior of T_C for small n is sensitive to the approximation. In the Hartree-Fock approximation, T_C should be finite for infinitesimal number of electron according to the Stoner condition $\rho(0)U > 1$ because the noninteracting DOS diverge at $n = 0$. This holds true even in the static approximation because the SA reduces to the Hartree-Fock approximation in the weak Coulomb interaction limit. The QMC results suggest that T_C vanish at finite electron number in the low density region. There is no exact analysis on the low-density behavior of T_C for this system as far as we know. The present calculations indicate that T_C vanishes at $n = 0.2$ for $U = 2$, and at $n = 0.3$ for $U = 4$.

Magnetic properties at the high temperatures above T_C are expected to be described well by the dynamical CPA+HA. We present in Figs. 11 and 12 calculated effective Bohr magneton number (m_{eff}) and amplitude of local moment ($\langle m^2 \rangle^{1/2}$) as a function of electron number n . Note that $\langle m^2 \rangle^{1/2} = \sqrt{3} \langle m^2 \rangle^{1/2}$ where $\langle m^2 \rangle^{1/2}$ is the

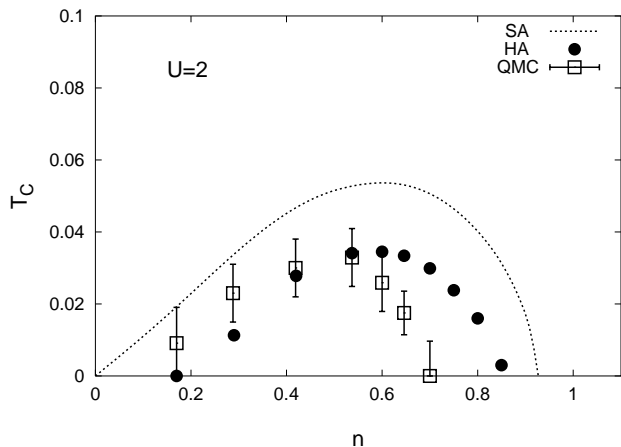


Fig. 9. Curie temperature (T_C) vs. electron number (n) at $U = 2$ in the SA (dotted curve), the HA (closed circles), and the QMC (open squares with error bars).³³⁾

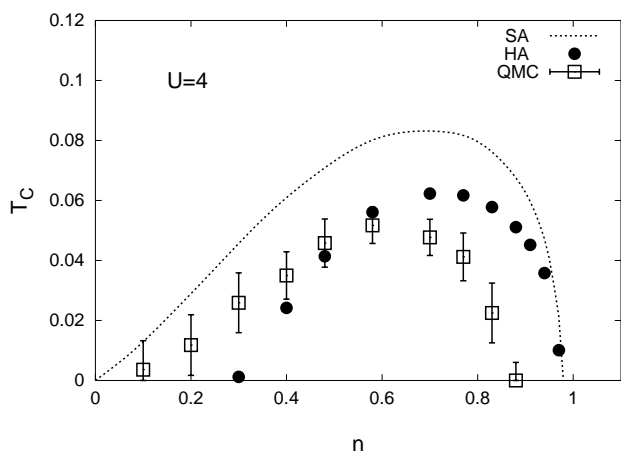


Fig. 10. Curie temperature vs. electron number at $U = 4$ in the SA (dotted curve), the HA (closed circles), and the QMC (open squares with error bars).³³⁾

amplitude of local moment for z component given by eq. (20). These quantities were obtained at high temperatures ($T \approx 0.09$). In the case of $U = 2$, the effective Bohr magneton number monotonically increases with increasing electron number from 0 to 1, and shows the maximum $1.64 \mu_B$ at half-filling. Although m_{eff} agrees with the amplitude $\langle \mathbf{m}^2 \rangle^{1/2}$ in the atomic limit, it is in general smaller than the latter in the metallic state. At half-filling, the difference is small; $m_{\text{eff}} \approx \langle \mathbf{m}^2 \rangle^{1/2}$ because of considerable suppression of charge fluctuations. By comparing the effective Bohr magneton numbers in the HA with those in the SA, we find that the dynamical effects enhance the effective Bohr magneton number, though the SA describes m_{eff} quantitatively at half-filling.

For larger value of $U = 4$, we find similar behavior of m_{eff} as a function of n , but the effective Bohr magneton number shows a maximum at $n \approx 0.95$, and jumps from $1.3 \mu_B$ to $1.6 \mu_B$ at $n = 1$. Sudden jump to the value $1.6 \mu_B$ being close to the atomic value $\sqrt{3}$ is associated with the formation of an insulator at half-filling. Calculated effective Bohr magneton number at $n = 0.58$ quantita-

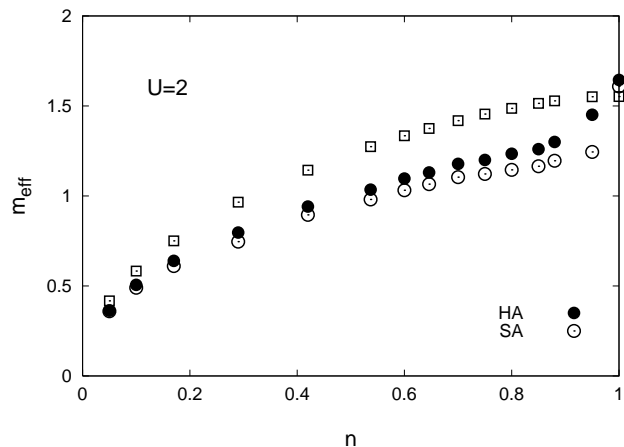


Fig. 11. Calculated effective Bohr magneton numbers (m_{eff}) as a function of the electron number n in the HA (closed circles) and in the SA (open circles). Coulomb interaction energy is fixed to be $U = 2$. The amplitudes of local moments $\langle \mathbf{m}^2 \rangle^{1/2}$ are also presented by open squares.

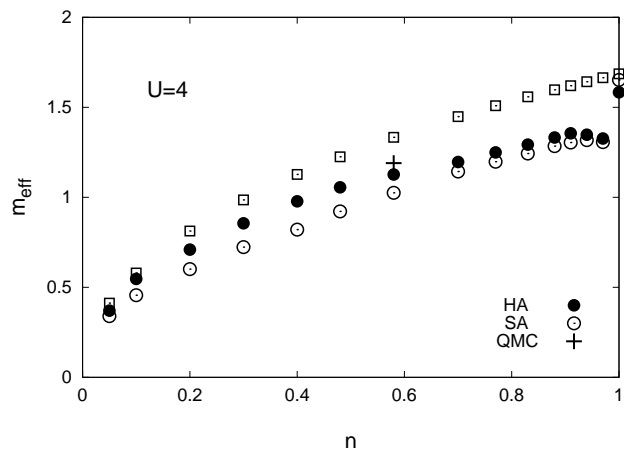


Fig. 12. Same as in Fig. 11 but for $U = 4$. The QMC result at $n = 0.58$ is shown by +.

tively agrees with the QMC result as shown in Fig. 12.

4. Summary

In the present paper we have investigated magnetic and electronic properties of the Hubbard model in infinite dimensions on the basis of the dynamical CPA combined with the harmonic approximation (HA) in order to clarify the accuracy of the theory at finite temperatures.

In the dynamical CPA, we transform the interacting electron system into an independent electron system coupled with the time-dependent random charge and exchange fictitious fields on the basis of the functional integral method. Introducing the coherent potential, we made a single-site approximation in the free energy. The coherent potential is self-consistently determined by the condition that the average of dynamical impurity Green function embedded in the effective medium (*i.e.*, the coherent potential) should be equal to the coherent Green function for the uniform medium. The former Green

function is calculated by means of the HA. The dynamical CPA+HA becomes exact in the high-temperature limit, leads to the free energy being exact up to the second order in the weak U limit, and yields the exact result in the strong U limit in infinite dimensions.

We have performed the numerical calculations with use of the dynamical CPA+HA in which the dynamical corrections have been taken into account up to the 4th order in U exactly and the higher-order corrections up to the 16th order in U have been taken into account with use of the second order asymptotic approximation. In the present calculations for the half-filled band Hubbard model on the Bethe lattice in infinite dimensions we found that the Néel temperatures T_N are well described by the zeroth approximation to the dynamical CPA, *i.e.*, the static approximation (SA). The dynamical corrections based on the HA reduce further T_N in the weak Coulomb interaction regime, leading to a quantitative agreement with the QMC results. In the intermediate Coulomb interaction regime, the dynamical corrections in the present approximation tend to underestimate T_N by about 10%. In the strong Coulomb interaction regime we found that the dynamical corrections slightly increase T_N . These results suggest that the dynamical CPA+HA can describe T_N within 10% error in infinite dimensions.

We have also verified using the same model at half filling that the SA quantitatively describes the MI crossover above T_N . It however underestimates the critical Coulomb interaction U_c at low temperatures. The dynamical corrections based on the HA enhance U_c . But the corrections in the present version are not enough to reproduce quantitatively the critical U_c obtained by the QMC; the present theory leads to U_c smaller than those of the QMC by 30% at low temperatures ($T \sim 0.02$).

We have investigated the ferromagnetic properties on the fcc lattice in infinite dimensions. In this case, the SA overestimates the Curie temperatures T_C more than 30% irrespective of electron number. The dynamical CPA+HA reduces T_C in the SA, and quantitatively describes the Curie temperatures as well as the susceptibilities in the quarter-filled regime ($0.4 \lesssim n \lesssim 0.6$). However the T_C vs n curves tend to shift to the higher density region by about $\Delta n = 0.1$ as compared with those in the QMC calculations, so that T_C in the low density region ($0 < n \lesssim 0.3$) are somewhat underestimated and those in the half-filled regime ($0.7 \lesssim n < 1$) are overestimated. We found that the effective Bohr magneton number m_{eff} is smaller than the amplitude $\langle m^2 \rangle^{1/2}$ in itinerant electron system except at half-filling where electrons tend to localize due to electron correlations for the intermediate Coulomb interaction strength. The dynamical effects enhance m_{eff} for non half-filled bands, while the corrections are negligible at half-filling.

We have to perform the full CPA calculations without decoupling approximation (21) in order to obtain more solid conclusions. Nevertheless, the present results of calculations indicate that the dynamical CPA combined with the HA is suitable for the quantitative calculations of magnetic properties at finite temperatures as well as the MI transition at high temperature region.

It is not enough for the quantitative description of the MI transition at low temperatures and for the quantitative description of the ferromagnetism in the low-density regime as well as in the half-filled regime. For more quantitative description in the intermediate Coulomb interaction and low-temperature regime, one has to treat more seriously the higher-order dynamical corrections. The improvement is left for future work.

Acknowledgment

One of the authors (T.T.) is grateful to Mr. T. Nakamura for valuable discussions on the densities of states in infinite dimensions. This work was partly supported by the Ministry of Education, Science, Sports and Culture, Grant-in-Aid for Scientific Research (C), 22540395, 2010. Numerical calculations have been partly carried out with use of the Hitachi SR11000 in the Supercomputer Center, Institute of Solid State Physics, University of Tokyo.

-
- 1) P. Fulde: *Electron Correlations in Molecules and Solids* (Springer Verlag, Pub., Berlin, 1995) Chap. 11.
 - 2) Y. Kakehashi: Adv. Phys. **53** (2004) 497; Phil. Mag. **86** (2006) 2603.
 - 3) M. Cyrot: J. Phys. (Paris) **33** (1972) 25.
 - 4) See for example, G. Morandi, E. Galleani, D'Agliano, F. Napoli, and C.F. Ratto: Adv. Phys. **24** (1974) 867.
 - 5) J. Hubbard: Phys. Rev. B **19** (1979) 26267; B **20** (1979) 4584; B **23** (1981) 5974.
 - 6) H. Hasegawa: J. Phys. Soc. Jpn **46** (1979) 1504; **49** (1980) 178.
 - 7) See for example, H. Ehrenreich and L.M. Schwartz: Solid State Phys. **31** (1976) 1.
 - 8) M.C. Gutzwiller: Phys. Rev. Lett. **10** (1963) 159; Phys. Rev. **134** (1964) A293; Phys. Rev. **137** (1965) A1726.
 - 9) J. Hubbard: Proc. Roy. Soc. (London) A **276** (1963) 238; A **281** (1964) 401.
 - 10) J. Kanamori: Prog. Theor. Phys. **30** (1963) 275.
 - 11) Y. Kakehashi and P. Fulde: Phys. Rev. B **32**, (1985) 1595.
 - 12) Y. Kakehashi: Phys. Rev. B. **45** (1992) 7196; J. Magn. Magn. Mater. **104-107** (1992) 677.
 - 13) Y. Kakehashi: Phys. Rev. B **65** (2002) 184420.
 - 14) D.J. Amit and C.M. Bender: Phys. Rev. B **4** (1971) 3115; D.J. Amit and H.J. Keiter: Low Temp. Phys. **11** (1973) 603.
 - 15) Dai Xianxi: J. Phys. Condens. Matter. **3** (1991) 4389.
 - 16) Y. Kakehashi: Phys. Rev. B **66** (2002) 104428.
 - 17) S. Hirooka and M. Shimizu: J. Phys. Soc. Jpn. **43**, (1977) 70.
 - 18) A. Georges, G. Kotliar, W. Krauth, M.J. Rosenberg: Rev. Mod. Phys. **68** (1996) 13.
 - 19) Y. Kakehashi and P. Fulde, Phys. Rev. B **69** (2004) 045101; Phys. Rev. B **70** (2004) 155112.
 - 20) Y. Kakehashi, T. Shimabukuro, T. Tamashiro, and T. Nakamura: J. Phys. Soc. Jpn. **77** (2008) 094706.
 - 21) O.K. Andersen: Phys. Rev. B **12** (1975) 3060.
 - 22) O.K. Andersen, O. Jepsen, and G. Krier: in *Methods of Electronic Structure Calculations* ed. by V. Kumar, O.K. Andersen, and A. Mookerjee (World Scientific Pub., Singapore, 1994) p. 63.
 - 23) V.I. Anisimov, F. Aryasetiawan, and A.I. Lichtenstein: J. Phys. Condens. Matter **9** (1997) 767.
 - 24) Y. Kakehashi, M.A.R. Patoary, and T. Tamashiro: J. Phys. Soc. Jpn. **78** (2009) 093705.
 - 25) Y. Kakehashi, T. Tamashiro, M.A.R. Patoary, and T. Nakamura: J. Phys.: Conference Series **200** (2010) 032030.
 - 26) Y. Kakehashi, M.A.R. Patoary, and T. Tamashiro: Phys. Rev. B **81** (2010) 245133.
 - 27) Y. Kakehashi and M.A.R. Patoary: J. Phys. Soc. Jpn. **80** (2011) 034706.

- 28) E. Müller-Hartmann: in Proc. V Symp. Phys. of Metals, ed. by E. Talik, J. Szade (Ustron-Jaszowiec, Poland, 1991) p. 22.
- 29) M. Ulmke, V. Janis, and D. Vollhardt: Phys. Rev. B **51** (1995) 10411.
- 30) K. Held, M. Ulmke, N. Blümer, and D. Vollhardt: Phys. Rev. B **56** (1997) 14469.
- 31) J. Schlipf, M. Jarrell, P.G.J. Dongen, N. Blümer, S. Kehrein, Th. Pruschke, and D. Vollhardt: Phys. Rev. Lett. **82** (1999) 4890.
- 32) G. Moeller, G. Kotliar, Q. Si, M. Rosenberg, and D.S. Fisher: Phys. Rev. Lett. **74** (1995) 2082.
- 33) M. Ulmke: Eur. Phys. J. B **1** (1998) 301.
- 34) J. Hubbard: Phys. Rev. Lett. **3** (1959) 77; R.L. Stratonovich: Dokl. Akad. Nauk. SSSR **115** (1958) 1097; Sov. Phys. Dokl. **2** (1958) 416.
- 35) E.-N. Foo and H. Amar: Phys. Rev. Lett. **25** (1970) 1748.
- 36) M. Plischke and D. Mattis: Phys. Rev. B **7** (1973) 2430.
- 37) Note that $\Delta T_N(\Delta U_c)$ is not caused by the decoupling approximation, but is caused by the dynamical corrections in eqs. (8) and (16).
- 38) H.J. Vidberg and J.W. Serene: J. Low Temp. Phys. **29** (1977) 179.
- 39) J. Koringa: J. Phys. Chem. Solids **7** (1958) 252.